Acoustically-Induced Water Frustration for Enhanced Hydrogen Evolution Reaction in Neutral Electrolytes

Yemima Ehrnst, Peter C. Sherrell, Amgad R. Rezk,* and Leslie Y. Yeo

A novel strategy utilizing high-frequency (10 MHz) hybrid sound waves to dramatically enhance hydrogen evolution reactions (HER) in notoriously difficult neutral electrolytes by modifying their network coordination state is presented. Herein, the practical limitations associated with existing electrolyzer technology is addressed, including the need for highly corrosive electrolytes and expensive electrocatalysts, by redefining conceptually-poor hydrogen electrocatalysts in neutral electrolytes. The improvement in HER performance is attributed to the unique capability of the intense local electromechanical coupling arising from the acoustic-forcing to 'frustrate' the tetrahedrally-coordinated hydrogen bond network of water molecules at the electrode–electrolyte interface, resulting in the generation of a high concentration of "free" water molecules that are more readily able to access catalytic sites on the unmodified polycrystalline electrode. Together with the other synergistic effects that accompany the acoustic excitation (e.g., hydronium ion generation, convective relaxation of diffusion mass transfer limitations, and prevention of bubble build-up and their removal from the electrode), the resultant overpotential reduction of 1.4 V at -100 mA cm^{-2} and corresponding 14-fold increase in current density, together with a net-positive energy saving of 27.3%, showcases the potential of the technology as a scalable platform for effectively enhancing the efficiency of green hydrogen production.

1. Introduction

Hydrogen (H_2) is set to be pivotal in the transition to a clean-energy economy as it provides a high-energy density carrier for

Y. Ehrnst, A. R. Rezk, L. Y. Yeo
Micro/Nanophysics Research Laboratory
School of Engineering
RMIT University
Melbourne, Victoria 3001, Australia
E-mail: amgad.rezk@rmit.edu.au
P. C. Sherrell
Department of Chemical Engineering
The University of Melbourne
Parkville, Victoria 3010, Australia

renewable energy.[1–3] Despite its appeal of green H_2 production using energy from renewable sources, water electrolysis currently only accounts for a small percentage of global H_2 production due to the need for expensive electrocatalysts to compensate for Ohmic losses associated with the kinetic overpotential of the system.[4–6] At present, H_2 production via electrolysis is predominantly carried out in strong acidic/alkaline electrolytes using state-of-the-art platinum group metal (PGM) electrocatalysts, which enables hydrogen evolution reactions (HER) to be conducted at the lowest onset potential, albeit at practically insurmountable industrial costs due to the metal's scarcity.[7,8] To attain industrially-relevant current densities (200–500 mA cm^{-2}), an overpotential between 1.8 and 2.5 V is typically required.[9] At these levels though, acidic electrolytes—while providing an abundant source of protons (H^+) and hydronium (H_3O^+) ions—produce acid fog under high temperatures that can corrode the electrolyzer and contaminate the product.[10] Alkaline electrolysis, on the other hand, is commonly plagued by unstable electrocatalysts and the need for expensive pH-tolerant membranes.[11–13]

It is therefore desirable to carry out electrolysis in neutral or near-neutral electrolytes (pH 5–9) with non-PGM electrocatalysts.[14] The HER rate under these conditions is, nevertheless, significantly lower than those for electrolytes with extreme pH levels. In addition to diffusion limitations, this is due to the rapid consumption of H_3O^+, which creates a bottleneck that limits the extent of reaction until higher overpotentials are able to drive H_2O reduction.[10,15–17] Even with the best electrodes (i.e., PGMs), H_2 production is several orders of magnitude lower under neutral conditions,[7] such that the overpotential required to reach a current density of -4 mA cm^{-2} exceeds 0.25 V in a 0.1 M $KClO_4$ electrolyte compared to as little as 30 mV in 0.5 M H_2SO_4.[18,19] Similarly poor performance is obtained with the use of nickel-based electrocatalysts, which are generally favored for alkaline conditions, given their affinity for OH^- adsorption.[20] To circumvent these limitations, novel electrocatalysts have been designed, in which the electrode is doped to tailor its catalytic sites for both H* and OH* adsorption to complement the electrolytic conditions,[21–23] or through the introduction of complex architectures that facilitate more favorable local pH environments,[24] although these strategies
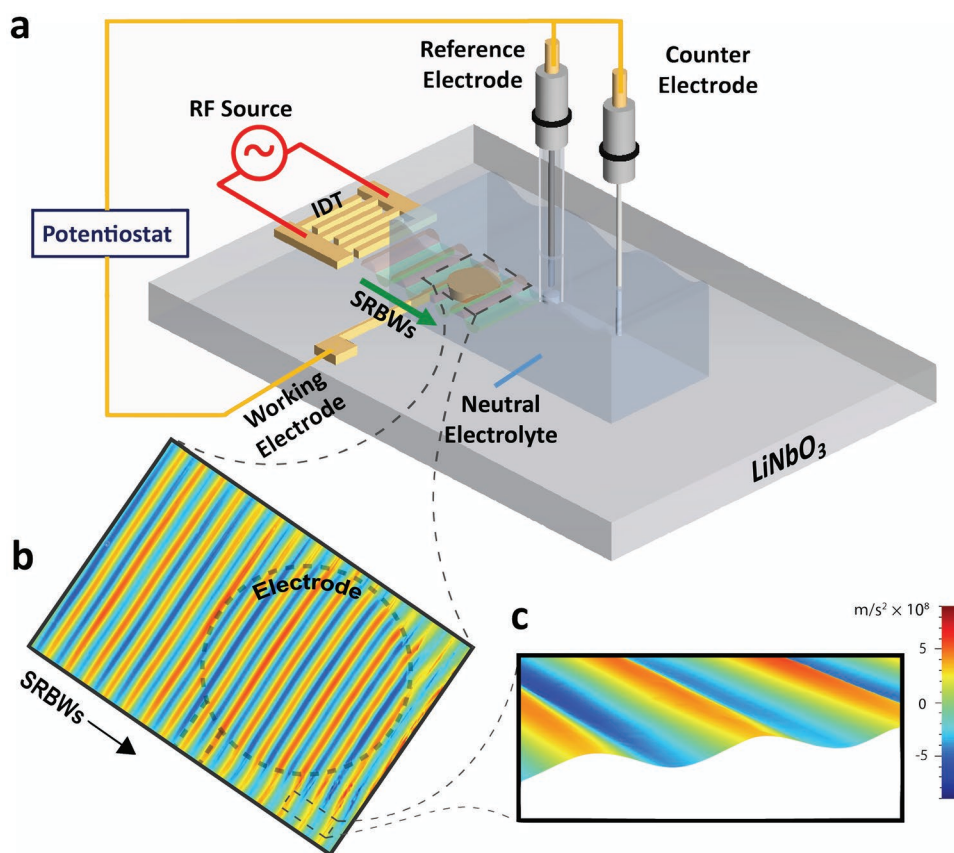
Figure 1. a) Schematic depiction (not to scale) of the SRBW electrochemical cell that consists of a glass electrolyte chamber containing the neutral electrolyte (0.1 M sodium phosphate; Na_2HPO/NaH_2PO_4) atop the chipscale SRBW device, which comprises a piezoelectric (lithium niobate; $LiNbO_3$) substrate on which an interdigital transducer (IDT) electrode is patterned. A circular polycrystalline gold (Au) working electrode (WE) is also patterned on the substrate in the SRBW propagation pathway beneath the chamber. The electrochemical setup is completed by an Ag/AgCl reference electrode (RE) and platinum (Pt) wire counter electrode (CE) mounted in the lid of the chamber. b,c) Laser Doppler vibrometry scans of the SRBWs (20 dBm) propagating on the $LiNbO_3$ substrate and through the WE (dashed outline); the color bar denotes the magnitude of the surface acceleration associated with the SRBW.

do not address the practical issue surrounding the costs of fabricating and engineering these specialized catalysts.

In this work, we demonstrate considerably enhanced HER performance in a neutral electrolyte (0.1 M sodium phosphate (Na_2HPO/NaH_2PO_4); pH 7.2) on polycrystalline gold (Au) electrodes (as confirmed by the x-ray diffraction pattern in Figure S1, Supporting Information) through the incorporation of nanoscale MHz-order electromechanical oscillations in the form of unique hybrid surface and bulk acoustic waves known as surface reflected bulk waves (SRBWs).[25] Au was intentionally chosen as the electrode material as it is a well-studied, stable but yet relatively poor performing HER catalyst, therefore allowing us to highlight the simple potential of the SRBWs in improving a generic catalyst.[18,26] The significant performance improvement that will be shown—an approximate 14-fold increase in current density as a consequence of the acoustic-forcing reducing the kinetic overpotential of the system—cannot be merely explained through conventional sonoelectrochemical mechanisms [27,28] that involve the use of lower frequency (20 kHz–3 MHz) bulk ultrasound to overcome diffusive mass transport limitations by inducing convective flow (acoustic streaming), and which therefore have

been limited to operation under acidic[29] and alkaline[30] conditions. That the higher MHz frequency excitation does not lead to the generation of cavitation bubbles[31] (unlike in conventional sonoelectrochemistry), in addition to being practically beneficial in reducing erosion and pitting of the electrodes, further reduces both diffusion limitations and Ohmic resistance due to bubble build-up at the electrodes, but is inadequate in itself to fully explain the order-of-magnitude improvement in performance observed.

Our investigations reveal a further dominant mechanism is at play: in the same way that the extraordinary surface acceleration ($\mathcal{O}(10^8$ m s^{-2})) (**Figure 1**b,c), local evanescent electric field ($\mathcal{O}(10^8$ V m^{-1})) and pressure ($\mathcal{O}(10^{-1}$–1 MPa)) associated with the SRBW-forcing has been shown previously to drive free radical and proton formation,[31,32] we show from an examination of the interfacial water structure via Raman spectroscopy, evidence for the disruption of the tetrahedral hydrogen bond water network of the neutral electrolyte. Such disruption creates a "frustrated" state comprising "free" water molecules with limited hydrogen bond coordination, whose reduced reorganization energy has been previously claimed to enhance the rate of electron transfer,[33–35] as well as HER kinetics, at least
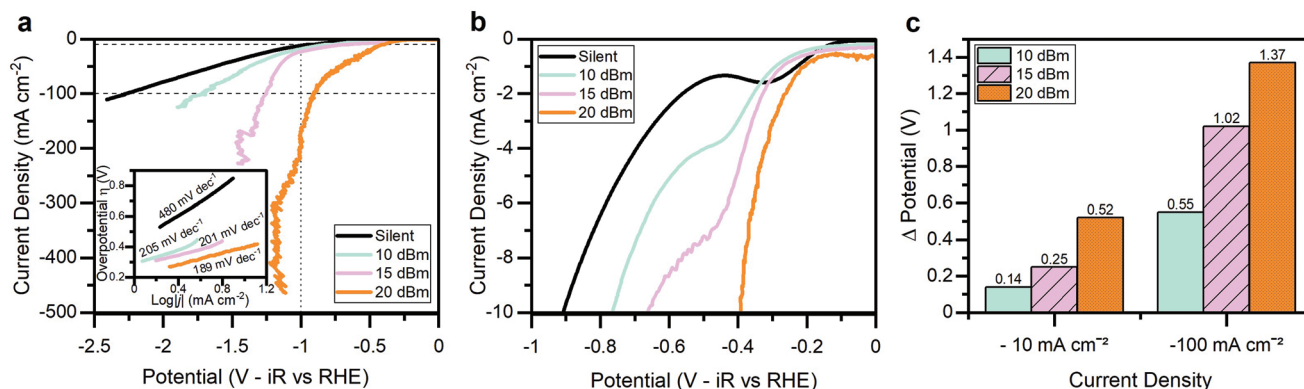
Figure 2. a,b) Linear sweep voltammograms (LSV) for HER in neutral 0.1 M Na_2HPO/NaH_2PO_4 electrolyte (pH 7.2) on polycrystalline Au under silent conditions as well as in the presence of the SRBW excitation at varying powers (10, 15, and 20 dBm); the inset in panel (a) plots the Tafel slopes for each of the respective conditions, showing a decrease in the slope with increasing SRBW power, whereas panel (b) is a magnification of the LSV in panel (a) in the low current density region, highlighting the existence of the switching plateau typical for neutral electrolytes due to the limited concentration of H^+ and H_3O^+ ions available at low applied potentials below the threshold at which water dissociates. c) Shift in the overpotential ΔV for the SRBW excited cases with varying power levels, with respect to that under silent conditions for two current densities (−10 mA cm^{-2} and −100 mA cm^{-2}).

in doped electrocatalytic systems in alkaline media,[36,37] and solely through the use of a different electrode material. While it has been shown that such "frustrated-water" states can be generated through nanoconfinement of water,[35] or through the application of intense electric[38–40] or pressure[41,42] fields, this first demonstration of frustrated water driven by vibration and its application for improving HER performance constitutes an integrable, net-positive energy-saving approach to neutral electrolysis and offers insight into in situ engineering of electrode–electrolyte interfaces for more efficient energy production.

2. Results and Discussion

Coupling the SRBW into the electrolysis cell using the custom-fabricated experimental setup depicted in Figure 1a (shown also in Figure S2, Supporting Information), a description of which can be found in the Methods Section of the Supporting Information, can be seen from the linear sweep voltammagram (LSV) in **Figure 2** to effectively decrease the overpotential compared to the "silent" (no SRBW-forcing) case (i.e., control). In particular, the Tafel plot in the inset of Figure 2a reveals a significant decrease in the Tafel slope from 0.480 V dec^{-1} under silent conditions to 0.205, 0.201, and 0.184 V dec^{-1} with the SRBW at 10, 15, and 20 dBm, respectively.[18,37,43] The extent to which the overpotential is reduced with the SRBW, can be observed from Figure 2c to be 0.52 and 1.37 V for current densities of −10 and −100 mA cm^{-2}, respectively. More specifically, with 20 dBm SRBW, the system requires a 0.2 V overpotential to reach a current density of −1 mA cm^{-2} (Figure 2b), which is lower than the 0.3–0.5 V[17] expected for neutral electrolytes with similar molarities. For −10 mA cm^{-2}, the requisite overpotential of 0.4 V is approximately half of that reported for platinum (Pt) in neutral electrolytes,[18,44] suggesting that SRBW-energized Au electrodes have superior performance to even Pt electrodes under neutral conditions. From another perspective, it can be seen that at −1 V, the current density increases by ≈14-fold (1290%) with the SRBW excitation, from −11.8 to −164.4 mA cm^{-2}.

Moreover, we note that under SRBW excitation, it is possible to achieve industrial current densities (−200—500 mA cm^{-2}) with the neutral electrolyte, which is not often reported in the literature.[6]

The aforementioned effect is neither limited to the electrolyte nor the electrode material. Under alkaline conditions (0.1 M KOH electrolyte; pH 13), for example, the LSV curves in Figure S3a,b shows that a shift in the overpotential of 0.38 and 1.05 V at −10 and −100 mA cm^{-2}, respectively, and an ≈32-fold improvement in current density at 0.75 V, which is comparable to the enhancement seen above for neutral electrolytes. In addition, a similar offset in the current density with SRBW excitation is observed, and the Tafel slopes in Figure S3c (Supporting Information) appear to also follow the same trend as that obtained for the neutral electrolyte. Likewise, experiments performed using silver as the working electrode instead of gold, which also performs poorly unless modified[45] or pre-treated,[46] yield similar increases in electrocatalytic performance and trends under the SRBW excitation, namely a reduction in the overpotential coupled with an increase in current density (Figure S4, Supporting Information).

It is likely that the SRBW facilitates such remarkable enhancement in the HER performance not just through a single mechanism, but through its effect in reducing each of the overpotential contributions that make up the total overpotential of the system:

$$\eta_{total} = \eta_{act} + \eta_\Omega + \eta_{conc} \tag{1}$$

wherein η_{act} comprises the activation overpotential that governs the kinetics of the reaction, η_Ω the Ohmic overpotential that accounts for the electrical resistance of the cell, and η_{conc} the overpotential associated with the mass transport limitations in the system.[4,47] In neutral electrolytes, the factors that typically influence each of these overpotential contributions in strongly acidic or alkaline electrolytes, namely, the availability of catalytic sites, the existence of the diffusion layer, the propensity of the bubbles to hinder ion migration, and supersaturation effects that arise due to the growth of the bubbles,[47] are

known to be considerably amplified.[4] While determining the relative magnitude of the overpotential contributions is complex due to their interdependence, we discuss here the possible ways by which the SRBW can influence each contribution individually, noting that the effect of SRBW-heating can be ruled out given the absence of any noticeable changes in the LSV plot (Figure S5, Supporting Information). Additionally, we also confirm that the improvement in HER that is observed is not a result of dissolution of the Pt counter electrode and deposition on the polycrystalline Au working electrode.[48] Besides the absence of any evidence of Pt deposition on the Au working electrode, as confirmed from the X-ray photoelectron spectroscopy (XPS) measurements on the electrode in Figure S6 (Supporting Information), similar performance enhancements were noted with the SRBW excitation when the Pt counter electrode was replaced with Au foil (Figure S7, Supporting Information). In any case, we note that in contrast to acidic and alkaline conditions,[49–51] variations in HER performance due to Pt deposition only become apparent in neutral electrolytes after several hundred cycles,[52] i.e., timescales much longer than those over which the LSVs were conducted (typically 3 min), and leads to improvements in HER that are far lower than those observed in the present work with the SRBW forcing.

At low current densities prior to the onset of bubble nucleation, η_{act} is typically dominant given that the electrolytic reaction proceeds at levels which allow ions to diffuse to/from the bulk electrolyte. In this case, it is likely that the SRBW's ability to generate H^+ and H_3O^+ due to its large evanescent electric field ($\mathcal{O}(10^8$ V m^{-1})) associated with the electromechanical coupling in the substrate,[31] which exceeds the threshold intensity for self-ionization of pure water at least in the highly polarized regions defined by its nanoscale amplitudes,[31] is a prominent factor that leads to a substantial reduction in η_{act}. This is substantiated by the disappearance of the plateau[53] observed at ≈ −0.4 V in Figure 2b with increasing SRBW power, therefore confirming the existence of localized acidic environments due to H^+ and H_3O^+ generation.[54]

On the other hand, η_Ω and η_{conc} dominate at high current densities due to the build-up of bubbles that act to block the electrode.[47] In this case, the effect of the SRBW excitation on the reduction of these overpotential components predominantly arises as a consequence of the acoustic streaming (i.e., bulk liquid recirculation) it generates, which, in turn, 1) overcomes diffusive mass transfer limitations by compressing the diffusion layer,[54] and, 2) facilitates the detachment and removal of bubbles produced that would otherwise have been trapped at the electrodes. In the former, the effect of the SRBWs on η_Ω is evidenced by the uncompensated resistance values R_u (Table S1, Supporting Information) obtained from the Nyquist plots, from which an increase in the SRBW power can be seen to decrease R_u by 9.3% (10 dBm), 39.3% (15 dBm) and 57.8% (20 dBm) compared to silent conditions, therefore implying faster charge transfer and higher Faradaic efficiency[55] under the SRBW excitation. In the latter, it can be seen from **Figure 3** that the bubbles produced at the electrodes, which would otherwise have grown under silent conditions to a critical size (≈450 μm in the images shown) prior to their detachment from the surface when their buoyancy begins to exceed the adhesion force, were

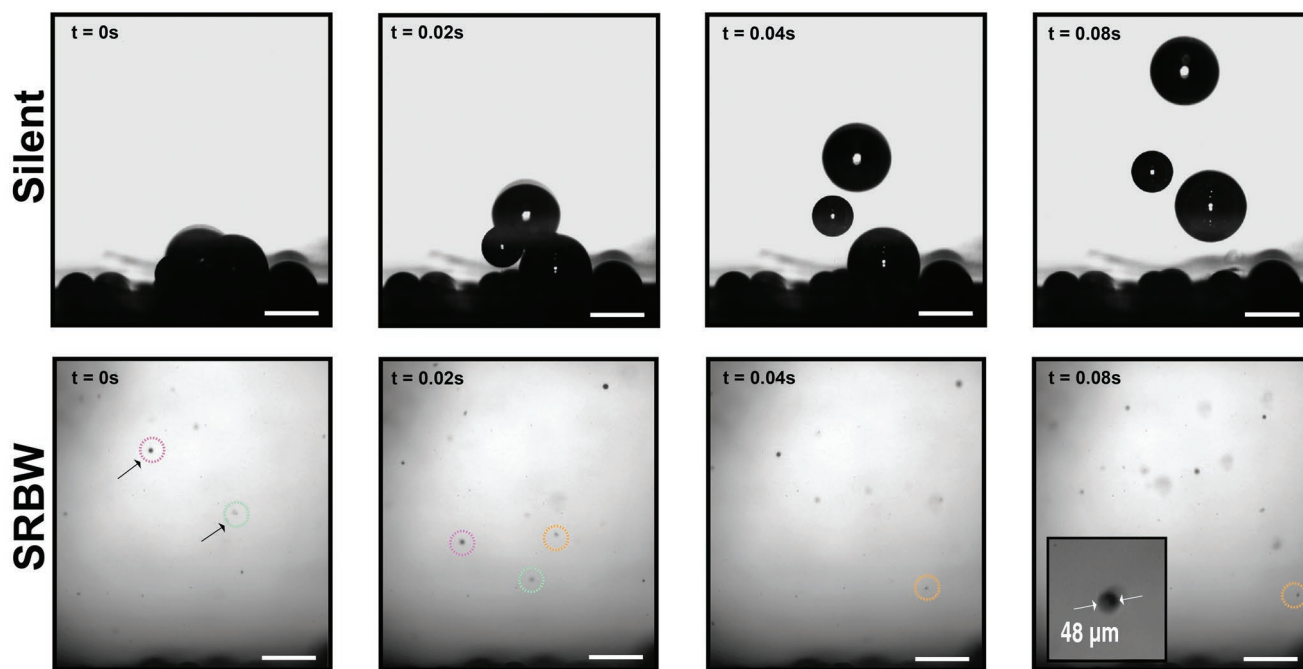**Figure 3.** Representative time series images acquired using a high speed camera (10 000 frames s^{-1}) showing the growth of bubbles trapped at the electrodes under silent conditions (top row), and under SRBW excitation at 20 dBm (bottom row). It can be seen that the bubbles produced under silent conditions grow to a critical size of ≈450 μm before detaching and lifting off the surface, whereas those under SRBW excitation are rapidly removed before they can grow further; the magnified image in the inset of the last panel shows the typical size (≈40 μm) to which bubbles grow under SRBW excitation before they are sheared off the electrode surface due to the convective SRBW-driven acoustic streaming flow. Identical bubbles are labeled by circles of the same color and the scale bars denote a length of 500 μm.

**ADVANCED
SCIENCE NEWS**

www.advancedsciencenews.com
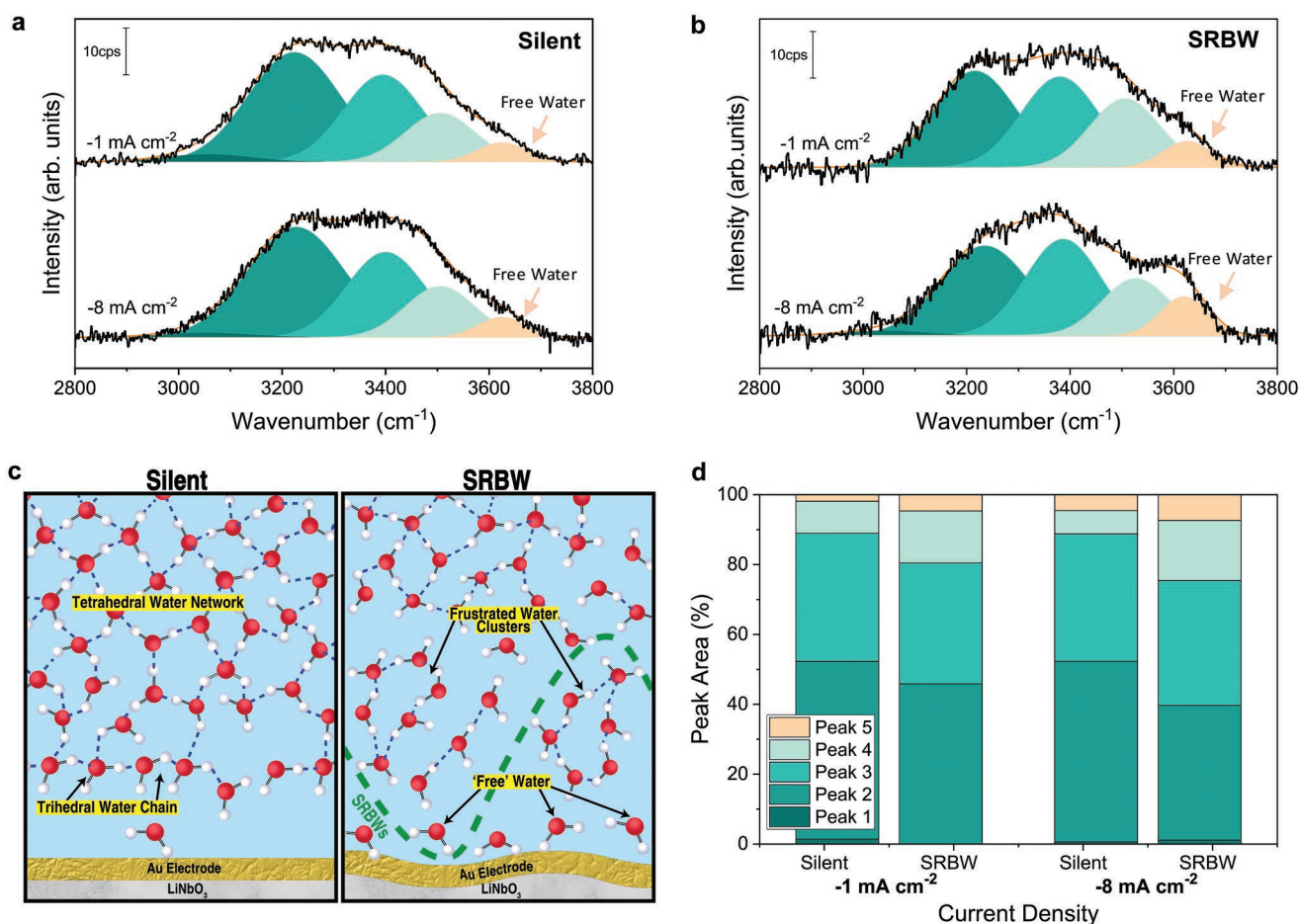
**ADVANCED
ENERGY
MATERIALS**

www.advenergymat.de

Figure 4. a,b) Deconvoluted Raman spectra associated with the hydrogen bond region describing the interfacial water state at the electrode–electrolyte interface under a) silent conditions, and b) SRBW excitation (15 dBm) in 0.1 M Na_2HPO/NaH_2PO_4 electrolyte for two current densities i.e., at low over-potentials and that just prior to bubble generation (−1 and −8 mA $cm^{−2}$, respectively). cps: counts per second. c) Schematic illustration of the interfacial water state at the electrode–electrolyte interface under silent (left panel) conditions in which the majority of water molecules (H: white; O: red) form a coordinated hydrogen bond (dashed blue lines) network of tetrahedral structures, in contrast to the corresponding state under SRBW excitation (right panel) wherein the coordination is disrupted to produce a "frustrated" state of trihedral water clusters as well as "free" water molecules, which more freely adsorbed onto the electrode (Au) surface. d) Bar plots of the relative areas under each deconvoluted peak, showing the existence of more "free" water as indicated by the fifth peak (shaded orange) due to the ability of the SRBW to disrupt the coordinated hydrogen bond network.

rapidly removed by the drag exerted by the SRBW-induced convective acoustic streaming flow before they have an opportunity to grow and coalesce, in sharp contrast to that observed with conventional sonoelectrochemistry.[29] As seen from Figure 3, the critical bubble size prior to detachment in the case of the SRBW excitation was typically an order-of-magnitude smaller (≈40 μm)—such early bubble removal and coalescence suppression then limits their build-up at the electrode, thus reducing both the electrical resistance as well as the diffusion barrier posed by the bubbles. These, in turn, facilitate easier access of the proton donors to the readily-available catalytic sites, leading to lower η_{conc}. Consequently, the electrolytic reaction under the SRBW was extremely stable, as confirmed by the chronopotentiometry results over 6 h in Figure S9. Moreover, the reduced bubble concentration to begin with, given that the SRBW does not generate cavitation[31] unlike in conventional sonoelectrochemistry,[56–58] and their early removal can be seen from Figure S10 (Supporting Information) to minimize electrode surface degradation due to bubble pitting.[59]

Interestingly, irrespective of these mechanisms (i.e., H^+ and H_3O^+ generation, convective relaxation of diffusive mass transfer limitations, and suppression of bubble growth and coalescence in addition to bubble removal from the electrodes) by which the SRBW can be seen to increase the efficiency of the electrolytic process, we find compelling evidence of an additional mechanism at play. **Figure 4**a,b shows results from the Raman spectra across the wavenumber range 3000–3800 $cm^{−1}$ corresponding to the hydrogen bond structure of the water molecules at the electrode–electrolyte interface under both silent and in situ SRBW conditions. Gaussian peaks were deconvoluted at ≈3055, 3230, 3392, 3520, and 3624 $cm^{−1}$, with lower wavenumbers (<3400 $cm^{−1}$) associated with rigid water molecules that are strongly bound within a tetrahedral network structure (Figure 4c, left panel), higher wavenumbers (>3400 $cm^{−1}$) associated with water molecules that are weakly bound within a trihedrally-coordinated structure; and the peak at 3624 $cm^{−1}$ specifically corresponding to "free" water molecules that do not participate in the hydrogen bond network

**ADVANCED
SCIENCE NEWS**

www.advancedsciencenews.com

**ADVANCED
ENERGY
MATERIALS**

www.advenergymat.de

(Figure 4c, right panel).[60] As can be seen by the the fitted peaks at −1 and −8 mA cm⁻² in Figure 4a, there is a modest increase in weakly-coordinated molecules (Peaks 4 and 5) under the silent condition. In stark contrast, the SRBW irradiation appeared to substantially enhance the concentration of these weakly-coordinated molecules, both at low overpotentials (at −1 mA cm⁻²) and at overpotentials just prior to significant bubble generation (at −8 mA cm⁻²) (Figure 4b). This enhancement can be seen in Figure 4d, which quantifies the area under each peak to show the relative concentrations of the different hydrogen bond network configurations. In particular, we observe the concentration of "free" water molecules, which is captured by the area under Peak 5, to increase substantially by 61.3% with SRBW excitation at −8 mA cm⁻², while Peak 2, which represents water molecules in a rigid tetrahedral configuration, can be seen to decrease by 25.4%. When considering both weakly-coordinated and "free" water collectively (Peaks 4 and 5), we thus observe the proportion of "frustrated" water to roughly double from 11.2% under silent conditions to 24.6% under the SRBW excitation for a current density of −8 mA cm⁻².

The implications of this finding should not be understated, given that water is more easily dissociated the weaker its coordination.[36] As illustrated in Figure 4c, "free" water molecules are able to more freely adsorb onto catalytic sites on the electrode compared to coordinated water molecules. As such, the activation energy for water dissociation decreases considerably for trihedrally-coordinated water compared to its tetrahedral counterpart, with "free" water having the lowest activation energy.[36,61] Consequently, it has been suggested that disruption of the tetrahedral hydrogen bond network can, in principle, reduce the overpotential to effect enhancements in the HER rate by facilitating easier and more effective mass transport of the water molecules through the Debye layer.[35,37,38,40–42,61,62] For example, it has been reported that an increase in the proportion of "frustrated" water of as little as 11%, which is similar to the 13.4% increase under the SRBW excitation observed here, was sufficient to result in an order-of-magnitude enhancement in current density[36,37] (cf. 14-fold enhancement obtained in the present work).

That the SRBW excitation is able to "frustrate" the hydrogen bond network of the interfacial water sufficiently to allow for dissociation of H-donors at lower overpotentials, thereby accelerating the HER rate, is perhaps not surprising in light of previous findings that such sound wave excitation, due to its intense surface mechanical ($\mathcal{O}(10^8$ m s⁻²)), electric ($\mathcal{O}(10^8$ V m⁻¹)) and pressure ($\mathcal{O}(10^{-1}$–1 MPa)) fields, is capable of breaking intramolecular (O–H) covalent bonds to dissociate the water molecules themselves,[31] which requires considerably more energy (492.2 kJ mol⁻¹[63]) than that to break the intermolecular coordination hydrogen bonds between the water molecules (23.3 kJ mol⁻¹).[64] To further isolate the effect of the SRBW on interfacial water orientation and to negate the possibility of any potential confounding effects arising from the presence of the buffer cations (Na⁺), which have also been known to influence higher wavenumber peaks,[37] we examined similar Raman spectroscopy measurements over the same wavenumber range (3000–3800 cm⁻¹) and LSVs under both silent and SRBW conditions for purified deionized water as the electrolyte instead (Figures S11 and S12, Supporting

Information). The percentage of "free" water in the case of the deionized water electrolyte was, however, considerably higher compared to that for the 0.1 M Na₂HPO/NaH₂PO₄ electrolyte, suggesting that the increased ionic strength in the latter partially screens the SRBW evanescent electric field and therefore suppresses its ability to drive further frustration in the intermolecular water network.

3. Conclusion

We show that the incorporation of high frequency hybrid acoustic wave excitation in the water electrolysis process is capable of substantially increasing the rate of the hydrogen evolution reaction by more than an order of magnitude, particularly for the more difficult case of neutral media, with simply a polycrystalline Au or Ag electrode and hence without the need for complex and expensive electrocatalysts. The reduction in overpotential and corresponding increase in current density obtained with the SRBWs compared to the control (silent) case is attributed to a combination of synergistic effects facilitated by the SRBW excitation. Namely, its ability to 1) "frustrate" the hydrogen bond coordination network of interfacial water to enable ease of accessibility to the electrode with the "free" water molecules, 2) generate H⁺ and H₃O⁺ ions in situ, and, 3) produce a strong convective flow, which not only i) overcomes diffusion mass transfer limitations, but also ii) facilitates increased electron transfer rates, and iii) rapidly removes bubbles from the electrode surface before they can grow further and coalesce. Given the efficiency by which the sound waves are coupled into the liquid phase through a chipscale device,[65–67] the mW power consumption required to generate the SRBW at the highest intensity (20 dBm) demonstrates a net energy saving of 27.3% (see Supporting Information). This is larger than the energy efficiencies (5–25%) reported with conventional sonoelectrochemistry, although we note that these studies[27,68,69] were performed under alkaline conditions in contrast to the more difficult case here of neutral electrolytes. As the current density of −100 mA cm⁻² obtained for silent conditions was only limited by the maximum value measurable with the potentiostat that was used, we expect the possibility for even greater relative enhancement with higher current densities, therefore highlighting the promise of this novel and potentially scalable (through massive parallelization of the low-cost SRBW devices by exploiting the economies-of-scale associated with mass nanofabrication[70]) approach as a practical and inexpensive means for green hydrogen production using generic, cheap, and traditionally-inferior electrode materials.

Supporting Information

Supporting Information is available from the Wiley Online Library or from the author.

Acknowledgements

Conflict of Interest

The authors declare no conflict of interest.

Data Availability Statement

The data that support the findings of this study are available from the corresponding author upon reasonable request.

[1] S. van Renssen, *Nat. Clim. Change* **2020**, *10*, 799.
[2] T. Egeland-Eriksen, A. Hajizadeh, S. Sartori, *Int. J. Hydrog. Energy* **2021**, *46*, 31963.
[3] L.-N. Zhang, R. Li, H.-Y. Zang, H.-Q. Tan, Z.-H. Kang, Y.-H. Wang, Y.-G. Li, *Energy Environ. Sci.* **2021**, *14*, 6191.
[4] C. Xiang, K. M. Papadantonakis, N. S. Lewis, *Mater. Horiz.* **2016**, *3*, 169.
[5] Z. P. Ifkovits, J. M. Evans, M. C. Meier, K. M. Papadantonakis, N. S. Lewis, *Energy Environ. Sci.* **2021**, *14*, 4740.
[6] Y. Xu, C. Wang, Y. Huang, J. Fu, *Nano Energy* **2021**, *80*, 105545.
[7] N. Mahmood, Y. Yao, J.-W. Zhang, L. Pan, X. Zhang, J.-J. Zou, *Adv. Sci.* **2018**, *5*, 1700464.
[8] Z. Pu, T. Liu, G. Zhang, Z. Chen, D.-S. Li, N. Chen, W. Chen, Z. Chen, S. Sun, *Adv. Energy Mater.* **2022**, *12*, 2200293.
[9] Y. Luo, Z. Zhang, F. Yang, J. Li, Z. Liu, W. Ren, S. Zhang, B. Liu, *Energy Environ. Sci.* **2021**, *14*, 4610.
[10] Z. Zhou, Z. Pei, L. Wei, S. Zhao, X. Jian, Y. Chen, *Energy Environ. Sci.* **2020**, *13*, 3185.
[11] T. Naito, T. Shinagawa, T. Nishimoto, K. Takanabe, *ChemSusChem* **2020**, *13*, 5921.
[12] C. Hu, L. Zhang, J. Gong, *Energy Environ. Sci.* **2019**, *12*, 2620.
[13] Z. Li, W. Niu, Z. Yang, A. Kara, Q. Wang, M. Wang, M. Gu, Z. Feng, Y. Du, Y. Yang, *Energy Environ. Sci.* **2020**, *13*, 3110.
[14] X. Wu, S. Zhou, Z. Wang, J. Liu, W. Pei, P. Yang, J. Zhao, J. Qiu, *Adv. Energy Mater.* **2019**, *9*, 1901333.
[15] T. Shinagawa, K. Takanabe, *Phys. Chem. Chem. Phys.* **2015**, *17*, 15111.
[16] K. E. Clary, M. Karayilan, K. C. McCleary-Petersen, H. A. Petersen, R. S. Glass, J. Pyun, D. L. Lichtenberger, *Proc. Natl. Acad. Sci. USA* **2020**, *117*, 32947.
[17] O. Jung, M. N. Jackson, R. P. Bisbey, N. E. Kogan, Y. Surendranath, *Joule* **2022**, *6*, 476.
[18] D. Strmcnik, M. Uchimura, C. Wang, R. Subbaraman, N. Danilovic, D. Van Der Vliet, A. P. Paulikas, V. R. Stamenkovic, N. M. Markovic, *Nat. Chem.* **2013**, *5*, 300.
[19] J. N. Hansen, H. Prats, K. K. Toudahl, N. Mørch Secher, K. Chan, J. Kibsgaard, I. Chorkendorff, *ACS Energy Lett.* **2021**, *6*, 1175.
[20] J. Kim, H. Jung, S.-M. Jung, J. Hwang, D. Y. Kim, N. Lee, K.-S. Kim, H. Kwon, Y.-T. Kim, J. W. Han, J. K. Kim, *J. Am. Chem. Soc.* **2020**, *143*, 1399.
[21] C.-T. Dinh, A. Jain, F. de Arquer, P. De Luna, J. Li, N. Wang, X. Zheng, J. Cai, B. Z. Gregory, O. Voznyy, B. Zhang, M. Liu, D. Sinton, E. J. Crumlin, E. H. Sargent, *Nat. Energy* **2019**, *4*, 107.
[22] Y.-Y. Ma, Z.-L. Lang, L.-K. Yan, Y.-H. Wang, H.-Q. Tan, K. Feng, Y.-J. Xia, J. Zhong, Y. Liu, Z.-H. Kang, Y.-G. Li, *Energy Environ. Sci.* **2018**, *11*, 2114.
[23] S. Chandrasekaran, M. Khandelwal, F. Dayong, L. Sui, J. S. Chung, R. Misra, P. Yin, E. J. Kim, W. Kim, A. Vanchiappan, Y. Liu, S. H. Hur, H. Zhang, C. Bowen, *Adv. Energy Mater.* **2022**, *12*, 2200409.
[24] H. Tan, B. Tang, Y. Lu, Q. Ji, L. Lv, H. Duan, N. Li, Y. Wang, S. Feng, Z. Li, C. Wang, F. Hu, Z. Sun, W. Yan, *Nat. Commun.* **2022**, *13*, 1.
[25] A. R. Rezk, J. K. Tan, L. Y. Yeo, *Adv. Mater.* **2016**, *28*, 1970.
[26] A. Goyal, M. T. Koper, *Angew. Chem. Int. Ed.* **2021**, *60*, 13452.
[27] M. H. Islam, O. S. Burheim, B. G. Pollet, *Ultrason. Sonochem.* **2019**, *51*, 533.
[28] J. Theerthagiri, J. Madhavan, S. J. Lee, M. Y. Choi, M. Ashokkumar, B. G. Pollet, *Ultrason. Sonochem.* **2020**, *63*, 104960.
[29] B. G. Pollet, F. Foroughi, A. Y. Faid, D. R. Emberson, M. H. Islam, *Ultrason. Sonochem.* **2020**, *69*, 105238.
[30] F. Foroughi, C. I. Bernäcker, L. Röntzsch, B. G. Pollet, *Ultrason. Sonochem.* **2022**, *84*, 105979.
[31] A. R. Rezk, H. Ahmed, T. L. Brain, J. O. Castro, M. K. Tan, J. Langley, N. Cox, J. Mondal, W. Li, M. Ashokkumar, L. Y. Yeo, *J. Phys. Chem. Lett.* **2020**, *11*, 4655.
[32] S. Wang, R. Herrmann, A. Reiner, A. Wixforth, C. Westerhausen, *Catal. Sci. Technol.* **2021**, *11*, 1458.
[33] R. C. Remsing, I. G. McKendry, D. R. Strongin, M. L. Klein, M. J. Zdilla, *J. Phys. Chem. Lett.* **2015**, *6*, 4804.
[34] D. T. Limmer, A. P. Willard, P. A. Madden, D. Chandler, *J. Phys. Chem. C* **2015**, *119*, 24016.
[35] R. K. Bhullar, M. J. Zdilla, M. L. Klein, R. C. Remsing, *J. Mater. Chem. A* **2021**, *9*, 6924.
[36] L.-F. Shen, B.-A. Lu, Y.-Y. Li, J. Liu, Z.-C. Huang-Fu, H. Peng, J.-Y. Ye, X.-M. Qu, J.-M. Zhang, G. Li, W.-B. Cai, Y.-X. Jiang, S.-G. Sun, *Angew. Chem. Int. Ed.* **2020**, *59*, 22397.
[37] Y.-H. Wang, S. Zheng, W.-M. Yang, R.-Y. Zhou, Q.-F. He, P. Radjenovic, J.-C. Dong, S. Li, J. Zheng, Z.-L. Yang, G. Attard, F. Pan, Z.-Q. Tian, J.-F. Li, *Nature* **2021**, *600*, 81.
[38] N. Garcia-Araez, V. Climent, J. Feliu, *J. Phys. Chem. C* **2009**, *113*, 9290.
[39] S. Floros, M. Liakopoulou-Kyriakides, K. Karatasos, G. E. Papadopoulos, *PloS One* **2017**, *12*, e0169505.
[40] M. Shafiei, N. Ojaghlou, S. Zamfir, D. Bratko, A. Luzar, *Mol. Phys.* **2019**, *117*, 3282.
[41] P. Postorino, M. Ricci, A. Soper, *J. Chem. Phys.* **1994**, *101*, 4123.
[42] R. Leberman, A. Soper, *Nature* **1995**, *378*, 364.
[43] We note that the values of the Tafel slopes are much higher than the theoretical value of either the Heyrovsky (40 mV dec^{-1}) or Tafel (30 mV dec^{-1}) steps, which is expected given the neutral electrolyte and the use of an Au working electrode[18,37].
[44] T. Shinagawa, A. T. Garcia-Esparza, K. Takanabe, *ChemElectroChem* **2014**, *1*, 1497.
[45] H.-J. Yin, J.-H. Zhou, Y.-W. Zhang, *Inorg. Chem. Front.* **2019**, *6*, 2582.
[46] J.-F. Huang, Y.-C. Wu, *ACS Sustain. Chem. Eng.* **2018**, *6*, 8285.
[47] A. Angulo, P. van der Linde, H. Gardeniers, M. Modestino, D. F. Rivas, *Joule* **2020**, *4*, 555.
[48] G. Jerkiewicz, *ACS Catal.* **2022**, *12*, 2661.

[49] J. Lee, J. H. Bang, *ACS Energy Lett.* **2020**, *5*, 2706.

[50] R. Chen, C. Yang, W. Cai, H.-Y. Wang, J. Miao, L. Zhang, S. Chen, B. Liu, *ACS Energy Lett.* **2017**, *2*, 1070.

[51] S. Mondal, S. K. De, R. Jana, A. Roy, M. Mukherjee, A. Datta, B. Satpati, D. Senapati, *ACS Appl. Energy Mater.* **2021**, *4*, 3017.

[52] L. Zhang, L. Han, H. Liu, X. Liu, J. Luo, *Angew. Chem. Int. Ed.* **2017**, *56*, 13694.

[53] The characteristic plateau in the current density is known to arise as a consequence of the exhaustion of available H$^+$ and H$_3$O$^+$ ions at low potentials until more can be produced upon dissociation of the water molecules at an applied potential beyond this value. We confirmed that this is the result of the limited availability of H$^+$ and H$_3$O$^+$ ions in the neutral electrolyte and not due to ion contamination introduced by the reference electrode by replacing the silver/silver chloride (Ag/AgCl) reference electrode with a mercury/mercury sulphate (Hg/HgSO$_4$) reference electrode, in which we observe the same plateau to persist (Figure S8, Supporting Information).

[54] M. Auinger, I. Katsounaros, J. C. Meier, S. O. Klemm, P. U. Biedermann, A. A. Topalov, M. Rohwerder, K. J. Mayrhofer, *Phys. Chem. Chem. Phys.* **2011**, *13*, 16384.

[55] H. Xu, G. Xu, L. Chen, J. Shi, *Adv. Mater.* **2022**, *34*, 2200058.

[56] C. C. Church, *Ultrasound Med. Biol.* **2002**, *28*, 1349.

[57] X. Zhao, R. Ranaweera, L. Luo, *Chem. Commun.* **2019**, *55*, 1378.

[58] The mechanical index[56]—a measure of the likelihood of cavitation events occurring due to acoustic irradiation—associated with the SRBW at the frequency and powers employed is still far lower by almost one order-of-magnitude even considering the decrease in the threshold for cavitation due to supersaturation of dissolved H$_2$ as a consequence of the high concentration of H$^+$ and H$_3$O$^+$ ions within proximity to the electrode.[57]

[59] F. Foroughi, J. J. Lamb, O. S. Burheim, B. G. Pollet, *Catalysts* **2021**, *11*, 284.

[60] C. C. Holzammer, A. S. Braeuer, *J. Phys. Chem. B* **2019**, *123*, 2354.

[61] Q. Wen, J. Duan, W. Wang, D. Huang, Y. Liu, Y. Shi, J. Fang, A. Nie, H. Li, T. Zhai, *Angew. Chem.* **2022**, *134*, e202206077.

[62] K. Sun, X. Wu, Z. Zhuang, L. Liu, J. Fang, L. Zeng, J. Ma, S. Liu, J. Li, R. Dai, X. Tan, K. Yu, D. Liu, W.-C. Cheong, A. Huang, Y. Liu, Y. Pan, H. Xiao, C. Chen, *Nat. Commun.* **2022**, *13*, 6260.

[63] O. V. Boyarkin, M. A. Koshelev, O. Aseev, P. Maksyutenko, T. R. Rizzo, N. F. Zobov, L. Lodi, J. Tennyson, O. L. Polyansky, *Chem. Phys. Lett.* **2013**, *568*, 14.

[64] S. Suresh, V. Naik, *J. Chem. Phys.* **2000**, *113*, 9727.

[65] J. Friend, L. Y. Yeo, *Rev. Mod. Phys.* **2011**, *83*, 647.

[66] J. Rufo, F. Cai, J. Friend, M. Wiklund, T. J. Huang, *Nat. Rev. Methods Primers* **2022**, *2*, 1.

[67] L. Y. Yeo, J. R. Friend, *Annu. Rev. Fluid Mech.* **2014**, *46*, 379.

[68] M.-Y. Lin, L.-W. Hourng, *J. Chin. Inst. Eng.* **2014**, *37*, 1080.

[69] C.-C. Wang, C.-Y. Chen, S.-D. Li, *Electrochim. Acta* **2009**, *54*, 3877.

[70] H. Ahmed, A. R. Rezk, J. J. Richardson, L. K. Macreadie, R. Babarao, E. L. Mayes, L. Lee, L. Y. Yeo, *Nat. Commun.* **2019**, *10*, 1.